Ultra-Widefield Indocyanine Green Angiography Reveals Patterns of Choroidal Venous Insufficiency Influencing Pachychoroid Disease

Tommaso Bacci,[1–3] Daniel J. Oh,[1,2,4,5] Michael Singer,[6] SriniVas Sadda,[7,8] and K. Bailey Freund[1,2,4,5]

[1]Vitreous Retina Macula Consultants of New York, New York, New York, United States
[2]Department of Ophthalmology, New York University Grossman School of Medicine, New York, New York, United States
[3]Ophthalmology Unit, Department of Medicine, Surgery and Neuroscience, University of Siena, Siena University Hospital, Siena, Italy
[4]LuEsther T. Mertz Retina Research Laboratory, Manhattan Eye, Ear and Throat Hospital, New York, New York, United States
[5]Columbia University Irving Medical Center, Edward S. Harkness Eye Institute, New York-Presbyterian Hospital, New York, New York, United States
[6]Medical Center of Ophthalmology, University of Texas Health Science Center, San Antonio, Texas, United States
[7]Doheny Eye Institute, Los Angeles, California, United States
[8]Ophthalmology, David Geffen School of Medicine, Los Angeles, California, United States

Correspondence: K. Bailey Freund, Vitreous Retina Macula Consultants of New York, 950 Third Ave, New York, NY 10022, USA; kbfnyf@aol.com.

Received: August 21, 2021
Accepted: December 21, 2021
Published: January 12, 2022

Citation: Bacci T, Oh DJ, Singer M, Sadda S, Freund KB. Ultra-widefield indocyanine green angiography reveals patterns of choroidal venous insufficiency influencing pachychoroid disease. *Invest Ophthalmol Vis Sci.* 2022;63(1):17. https://doi.org/10.1167/iovs.63.1.17

Purpose. To compare patterns of choroidal venous drainage in eyes with pachychoroid disease to those of healthy subjects using ultra-widefield indocyanine green angiography (UWF ICGA).

Methods. Patients with pachychoroid disease and healthy controls were recruited at two referral centers. UWF ICGA images were used to evaluate the proportion of the postequatorial fundus drained by major vortex vein systems in each quadrant and to study the incidence and topography of choroidal vascular hyperpermeability (CVH) and intervortex venous anastomoses. Widefield swept-source optical coherence tomography (SS-OCT) was used to evaluate choroidal thickness at the posterior pole in eyes with pachychoroid disease.

Results. Fifty-two pachychoroid eyes and 26 healthy eyes were evaluated. Eyes with pachychoroid disease showed a significant within-subject variance in the proportion of the postequatorial fundus drained by each vortex vein system (range, 4.1%–48.1%; $P < 0.0001$) that was not seen in controls (range, 17.3%–31.7%; $P = 0.11$). CVH was present in all pachychoroid disease eyes and three of 26 controls. Intervortex venous anastomoses were present in 46 of 52 pachychoroid disease eyes and nine of 26 control eyes. Vortex vein systems with large drainage areas showed greater density of CVH spots. SS-OCT demonstrated asymmetric choroidal drainage in the macula of 59% of pachychoroid eyes. CVH and intervortex venous anastomoses were more prominent in areas showing maximal choroidal thickness.

Conclusions. In eyes with pachychoroid disease, imbalanced choroidal venous drainage with congestion of specific vortex vein systems may contribute to a state of choroidal venous insufficiency characterized by regional choroidal thickening, CVH and remodeling of venous drainage routes.

Keywords: ultra-widefield indocyanine green angiography, pachychoroid disease, choroidal venous drainage, choroidal venous insufficiency

Pachychoroid disease as a nosological category was introduced several years ago to contextualize a *forme fruste* of central serous chorioretinopathy (CSC) characterized by retinal pigment epithelial abnormalities presenting in eyes with no history of subretinal fluid.[1] Subsequent observations contributed to further define a broader disease spectrum that includes CSC and other clinical presentations sharing imaging characteristics and alleged pathophysiology.[2–8]

The term "pachychoroid" contains an etymological reference to the supernormal choroidal thickness that has been reported in eyes with CSC using enhanced-depth imaging optical coherence tomography (EDI OCT)[9–12] and that appears to be a common feature of conditions within the pachychoroid disease spectrum. However, the diagnosis of pachychoroid disease cannot rely on a specific choroidal thickness value, because this parameter shows a great

Investigative Ophthalmology & Visual Science

intra-individual and interindividual variability and is influenced by multiple physiological and pathologic determinants.[13–16] Nevertheless, choroidal thickness measurements incongruous with values typical of a patient's demographics and ocular anatomy may be used diagnostically, especially in association with other characteristic multimodal imaging findings.[17,18] A relative choroidal thickening due to enlargement of deep choroidal veins may ultimately be implicated in mechanisms of inner choroidal and retinal pigment epithelium (RPE) damage[19–21] and is interpreted as a sign of choroidal venous congestion.

CSC pathophysiology as it relates to choroidal venous dysfunction dates back several decades when the use of indocyanine angiography (ICGA) was first introduced.[22–25] Iida et al. [26] and other collaborators described various choroidal alterations in eyes with pachychoroid disease including persistent vascular abnormalities, vascular remodeling with formation of intervortex venous anastomoses, and asymmetric choroidal venous drainage of the macular region.[21,27–31] The authors proposed that these alterations were consequences of impaired choroidal venous outflow, similar to what is seen in eyes with mechanical obstruction of vortex venous systems.[32]

The introduction of ultra-widefield (UWF) imaging has dramatically improved our ability to evaluate the far periphery of the fundus.[33,34] Specifically, UWF ICGA allowed for the first comprehensive in vivo visualization of the choroidal circulation, including the posterior pole and extending to and beyond the vortex vein ampullas.[35,36] Given this unique ability, this imaging technique has been applied to evaluate choroidal vascular changes in eyes with pachychoroid disease entities,[37–42] supporting the hypothesis that venous outflow congestion might be a possible contributing factor to the pathogenesis of this disease.[37]

The idea that pachychoroid disease is related to alteration of the choroidal venous homeostasis has gained consensus in the scientific community.[33] Nevertheless, the mechanisms by which venous congestion is produced in the choroid of eyes with pachychoroid disease remain poorly understood.

To explore possible mechanisms promoting a state of chronic choroidal venous insufficiency in pachychoroid disease, we compared patterns of choroidal venous drainage in eyes with various clinical manifestations within the pachychoroid disease spectrum to those of healthy subjects. By means of UWF ICGA and swept-source optical coherence tomography (SS-OCT), we evaluated the contribution of each vortex vein system to the overall postequatorial choroidal venous outflow and how the distribution of choroidal venous drainage by quadrant may affect the topography of biomarkers of pachychoroid disease, namely choroidal vascular hyperpermeability (CVH), intervortex venous anastomoses and choroidal thickness.

Methods

This was a retrospective observational study including electronic health records and multimodal imaging from pachychoroid patients seen by a single retina specialist (K.B.F.) at the Vitreous Retina Macula Consultants of New York, NY, USA, between February 2017 and January 2021 and from healthy controls recruited in a previously published study[35] at the Medical Center Ophthalmology Associates, San Antonio, Texas. The study design was approved by the Western Institutional Review Board (Olympia, WA, USA) and the Quorum Review IRB, complied with the Health Insurance Portability and Accountability Act of 1996 and followed the tenets of the declaration of Helsinki. Written informed consent was obtained from each participant.

Eyes of subjects with pachychoroid disease and eyes of healthy individuals represented the study and control group included in the present analysis, respectively. Patients were diagnosed as having pachychoroid disease if clinical and multimodal imaging demonstrated features consistent with one of the conditions within the pachychoroid disease spectrum in at least one eye. Diagnostic attributions were based on the recognition of specific characteristics for each pathologic entity,[17] associated with common findings that included (1) increased choroidal thickness co-localizing with areas of fundus abnormalities, (2) dilated choroidal vessels or reduced fundus tessellation in eyes with diffuse choroid thickening, (3) attenuation of the inner choroid in areas of fundus pathology, (4) ICGA choroidal hyperpermeability and reduced inner choroidal flow signal shown with OCTA, (5) dilated veins of Haller's layer ("pachyvessels") co-localizing with overlying disease manifestations, and (6) drusenoid RPE lesions or "pachydrusen." Patients with any other ocular or systemic condition possibly affecting the diagnostic accuracy were excluded, including any history of ocular trauma or posterior segment surgery, glaucoma filtration surgery, intraocular inflammation, extreme axial lengths (eyes with refractive error >6 diopters), choroidal masses including choroidal nevi, previous retinal laser photocoagulation or photodynamic therapy, use of non-antihypertensive vasodilator medications (e.g., phosphodiesterase inhibitors), uncontrolled diabetes or systemic hypertension and other systemic diseases possibly affecting the choroidal circulation, including Cushing syndrome.

All participants were evaluated with UWF ICGA using the Optos California (Optos PLC, Dunfermline, UK) system. UWF ICGA images were taken after intravenous injection of 25 mg of indocyanine green, during the early (up to two to three minutes after injection), middle (five to 10 minutes after injection), and late (10–20 minutes after injection) phases of the angiogram. One eye from each subject was included in the present analysis. The eye with the most salient clinical findings and the eye with more available early to mid-phase UWF ICGA images (the "transit eye") were selected for pachychoroid patients and healthy controls, respectively. Quantitative evaluation of the drainage areas of vortex vein systems, of CVH sites and of intervortex venous anastomoses was independently performed by two masked graders (T.B. and D.J.O.) to test reproducibility. The final consensus dataset was established after open adjudication when there was disagreement between the two graders.

Spectral-domain (SD) EDI-OCT and SS-OCT data were obtained in the pachychoroid cohort using the Spectralis HRA + OCT (Heidelberg Engineering GmbH, Heidelberg, Germany) and the PLEX Elite 9000 SS-OCT (software version 2.1.0.55513; Carl Zeiss Meditec, Inc., Dublin, CA, USA) systems, respectively.

Distribution of Choroidal Venous Drainage Into Quadrants

Early to mid-phase, macula-centered UWF ICGA images were selected from each case in the dataset. Images were rotated to place the main vortex veins at roughly at 45°, 135°, 225°, and 315°, and adjusted to obtain the most useful brightness/contrast ratio for visualization of major choroidal veins.

Investigative Ophthalmology & Visual Science

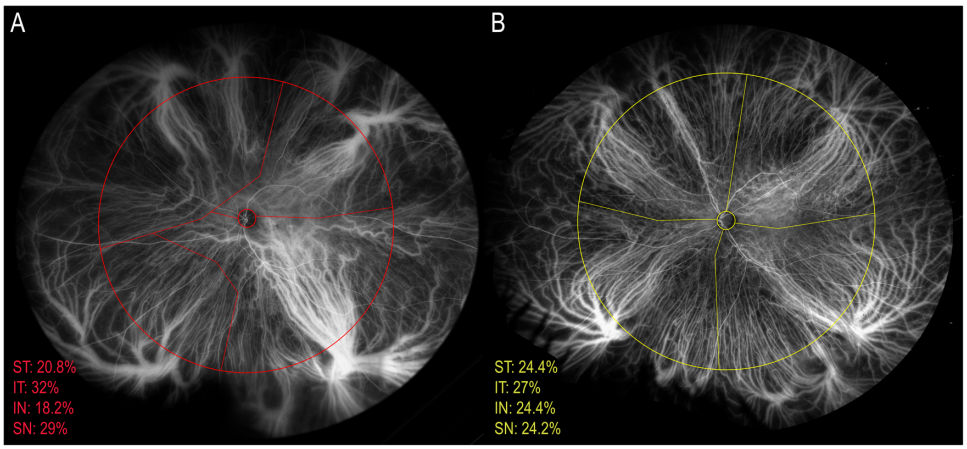

Figure 1. Early to mid-phase ultra-widefield indocyanine green angiography images of the left eye of a 70-year-old man with pachychoroid pigment epitheliopathy (**A**) and a 60-year-old healthy woman (**B**). The contribution to the overall postequatorial choroidal venous drainage of major vortex vein systems was measured as follows: the drainage area of each vortex vein system was manually demarcated (red and yellow markings for the pachychoroid disease and control eye, respectively) and expressed as a percentage of a circular area centered on the optic disc with its circumference intersecting the superotemporal vortex vein ampulla. Note that the choroidal venous drainage in the control eye (**B**) appears more evenly distributed into the 4 quadrants compared to the eye with pachychoroid pigment epitheliopathy (**A**). In the latter, the inferotemporal vortex vein drainage area is 32% of the postequatorial area including a large proportion of the peripapillary area and appears noticeably congested. In contrast, the inferonasal vortex vein drainage area is a relatively small portion of the postequatorial fundus (18.2%). ST, superotemporal vortex vein system drainage area; IT, inferotemporal vortex vein system drainage area; IN, inferonasal vortex vein system drainage area; SN, superonasal vortex vein system drainage area.

More than one image per eye was occasionally montaged together using Photoshop (version 21.1.3, Adobe, Inc., San Jose, CA, USA). To evaluate the contribution to the overall posterior choroidal venous drainage of major vortex vein systems located in the superotemporal (ST), inferotemporal (IT), inferonasal (IN), and superonasal (SN) quadrants, the drainage area of each vortex vein system, henceforth referred to as "VV drainage area," was manually demarcated using the polygon tool of the ImageJ software V.1.53c (National Institutes of Health, Bethesda, MD, USA; available at http://rsb.info.nih.gov/ij/index.html), and expressed as a percentage of the postequatorial fundus defined by a circular area centered on the optic disc, with the circumference intersecting the posterior margin of the ST vortex vein (Fig. 1).

Choroidal Venous Hyperpermeability and Intervortex Venous Anastomoses

The presence/absence of CVH in each eye, the total number of discrete CVH sites ("CVH spots") and the number of CVH spots corresponding to each VV drainage area were evaluated. CVH spots were defined as hyperfluorescent spots that could be clearly distinguished from the background fluorescence in mid-late ICGA images and that were associated with leakage phenomena not attributable to choroidal neovascularization. CVH spots with a greatest linear dimension ≤1 optic disc diameter were included in the quantitative analysis. Eyes presenting ill-defined or larger areas of mid-late hyperfluorescence were labeled as having "diffuse CVH." The topographic relation between CVH spots and VV drainage areas was evaluated after registration of mid-late and early ICGA images using the Register (Barycentric) ImageJ plugin (https://sites.imagej.net/CreativeComputation/plugins/CreativeComputation/).

The presence/absence of intervortex venous anastomoses in each eye, the total number of intervortex venous anastomoses and the number of intervortex venous anastomoses between the ST and IT, IT and IN, IN and SN, SN and ST vortex vein systems were manually counted. Intervortex venous anastomoses were defined as two anastomotic vessels connecting two separate vortex vein systems. To be included in the quantitative analysis, the connecting veins had to be greater than or equal to the size of a retinal arcade vein at the border of the optic disc.[43]

Choroidal Thickness Analysis

Subfoveal choroidal thickness was evaluated using the caliper tool of the Spectralis HRA + OCT viewing software (Heidelberg Engineering GmbH) on EDI SD-OCT B scans passing through the fovea. Widefield (≥9 × 9 mm) SS-OCT volume scans centered on the fovea were used to obtain choroidal thickness maps. Bruch's membrane and the choroid-scleral junction were set as segmentation boundaries. Sixteen-bit grayscale images (with each pixel value of the greyscale corresponding to a thickness value of the choroidal slab) were imported into ImageJ to perform quantitative measurements on custom-designed areas. Specifically, for each widefield SS-OCT scan, the mean choroidal thickness was calculated in the overall scanned area and in scanned areas corresponding to the drainage territories of the ST and IT vortex vein systems, as visualized using structural SS-OCT en face full-thickness choroidal slabs. SS-OCT en face projections and thickness maps of the choroid were manually registered to early and late phase UWF ICGA images to study the topographic relationship between CVH spots/intervortex venous anastomoses and choroidal thickness (Fig. 2).

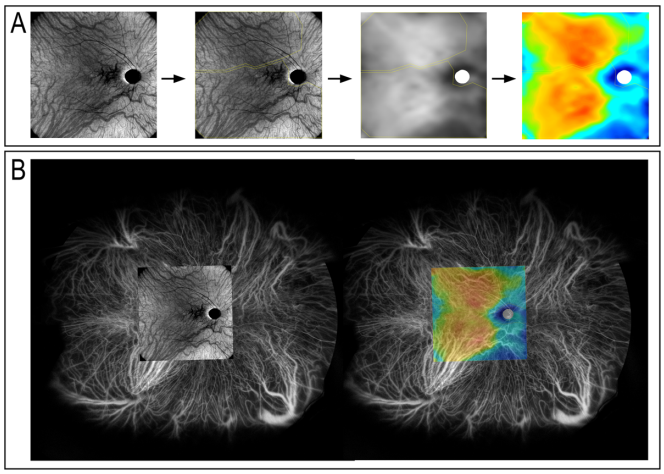

Figure 2. (**A**) Widefield (≥9 × 9 mm) SS-OCT volume scans centered on the fovea were used to obtain choroidal thickness maps. Sixteen-bit grayscale images (with each pixel value of the grayscale corresponding to a thickness value of the choroidal slab) were imported into ImageJ to perform quantitative measurements on custom-designed areas. The mean choroidal thickness was calculated in the overall scanned area and in areas corresponding to the drainage territories of the superotemporal and inferotemporal vortex vein systems, as visualized using structural SS-OCT en face projections segmenting the choroid. (**B**) SS-OCT en face projections and thickness maps of the choroid were manually registered to early and late phase ultra-widefield indocyanine green angiography images to study the topographic relationship between choroidal vascular hyperpermeability spots/intervortex venous anastomoses and choroidal thickness.

Statistics

Quantitative evaluation of VV drainage areas, CVH spots and intervortex venous anastomoses were tested for reproducibility using intraclass correlation coefficients (ICC). Normality assumption for all data was verified with the Shapiro-Wilk test. The independent-samples T-test and the Mann-Whitney U test were performed to assess the statistical significance of differences between groups for normally distributed and non-normally distributed variables, respectively. The Fisher exact probability test was applied in between-groups comparisons of categorical variables. Multiple linear regression models were used to test the effect of age, gender, and laterality on the size of each VV drainage area. Repeated-measure analysis of variance and the Friedman test were performed to analyze within-groups differences of VV drainage areas. The Spearman correlation was used to investigate the association of the VV drainage area with the number of intervortex venous anastomoses involving each vortex vein system and with the density of CVH spots in each VV drainage area. A level of <0.05 was set for statistically significance of P values. All statistical computations were performed using a commercially available statistical software (SPSS 25.0 for Windows; IBM Corp., Armonk, NY, USA).

Results

A total of 80 UWF ICGA studies of 80 pachychoroid patients were evaluated. Among those, 28 were excluded because early-phase images of the most affected eye had characteristics preventing reliable evaluation of venous drainage into different quadrants, including overall poor quality of the study (five cases), insufficient peripheral visualization (16 cases), presence of advanced RPE alterations affecting choroidal vein visualization (four cases), presence of posterior choroidal venous drainage routes (one case), and choroidal nevi (two cases). UWF ICGA images from 36 healthy subjects included in a previous study were made available to serve as controls in the present analysis.[35] Among those, 10 were excluded because their UWF ICGA studies had excessively fragmented views of the periphery, not allowing for a reliable evaluation of the choroidal circulation. A total of 52 pachychoroid eyes from 52 patients and 26 eyes from 26 healthy subjects were included in the present study. Clinical diagnoses in the pachychoroid disease group included pachychoroid pigment epitheliopathy in 11 eyes (21%), simple CSC[44] in 12 (23%), complex CSC[44] in 25 (48%), pachychoroid neovascularization in two cases, and aneurysmal type 1 macular neovascularization (AT1-MNV)/polypoidal choroidal vasculopathy (PCV) in two cases.

Twenty-six right eyes (OD) and 26 left eyes were included in the pachychoroid disease group, and 14 OD and 12 OS were included in the control group ($P = 0.81$). Groups were not matched for age and gender ($P < 0.0001$ and $P = 0.025$, respectively), with a lower mean age and fewer male subjects in the control group (47.5 ± 16.3 years [range, 21–76] and 42.3%, respectively) compared to the pachychoroid group (61.6 ± 10.8 years [range: 34–82] and 71.2%, respectively). Demographic and clinical characteristics of the pachychoroid disease group are listed in Table 1.

Distribution of Choroidal Venous Drainage Into Quadrants

Measurements of the VV drainage areas showed good reproducibility in each quadrant (Supplementary Table S1). Multiple linear regression models did not demonstrate significant effects of age, gender, and laterality on the size of the VV drainage areas in each quadrant (Supplementary Table S2). The median values of the ST, IT, IN, and SN VV drainage areas were 23.75 (interquartile range, 20.50–28.98), 26.00 (interquartile range, 22.77–29.27), 21.00 (interquartile range, 17.37–24.90), 28.85 (interquartile range, 24.57–32.92) and 24.88 (interquartile range, 23.40–26.65), 24.31 (interquartile range, 22.80–25-90), 24.65 (interquartile range,

Table 1. Demographic and Clinical Characteristics of the Pachychoroid Disease Group

Demographics	
Age (years, mean ± SD)	61.6 ± 10.8
Gender (M/F)	37 (71.2%)/15 (28.8%)
Medical history	
Hypertension	18
Diabetes mellitus	4
Coronary artery disease	2
Cardiac arrhythmias	0
Cardiomyopathy	0
Valvular heart disease	0
Cerebrovascular disease	0
Carotid artery disease	0
Sleep disorders/Obstructive sleep apnea	3
Chronic obstructive pulmonary disease	1
Chronic/recent corticosteroid use	1
Ocular history	
n° of evaluated eyes	52
Laterality (OD; OS)	26 (50%); 26 (50%)
Refractive error (SE, diopters; mean ± SD)	0.2 ± 0.9
Pseudophakic status	4
IOP lowering medications use	2

SD, standard deviation; M, male; F, female; OD, oculus dexter; OS, oculus sinister; SE, spherical equivalent; IOP, intraocular pressure.

23.30–25.82), 26.15 (interquartile range, 24.47–28.25) for the pachychoroid disease and the control group, respectively (Fig. 3). The pachychoroid group showed statistically significant within-subjects variance of drainage areas in each quadrant ($P < 0.0001$), whereas the control group did not ($P = 0.11$). The mean drainage area of the IN vortex vein system in the pachychoroid group was significantly smaller than in the control group ($P = 0.009$), whereas the mean SN VV drainage area was significantly larger ($P = 0.025$) (Table 2). In the pachychoroid disease group, the mean age of patients with at least one VV drainage area in the upper quartile range (29.47%–48.10%) (61.6 ± 10.5) was not significantly different compared to the mean age of the remainder cases (60.3 ± 11.8) ($P = 0.73$).

Choroidal Hyperpermeability and Intervortex Venous Anastomoses

Assessment of CVH presence/absence and the quantification of CVH spots in each VV drainage area showed good reproducibility (Supplementary Table S1). All 52 eyes in the pachychoroid group (100%) and three 26 control eyes (11.5%) demonstrated CVH in mid-late ICGA images ($P < 0.0001$) (Table 2). Four pachychoroid eyes demonstrated diffuse CVH and were subsequently excluded from quantitative analysis, which was then performed on a total of 48 pachychoroid eyes. Pachychoroid eyes showed a mean of 3.94 ± 3.5 CVH spots (range, 1–19). The mean number of CVH spots corresponding to the drainage areas of the ST, IT, IN, and SN vortex vein is shown in Table 2. Density of CVH spots (number of CVH spots corresponding to each VV drainage area/total VV drainage area) showed a

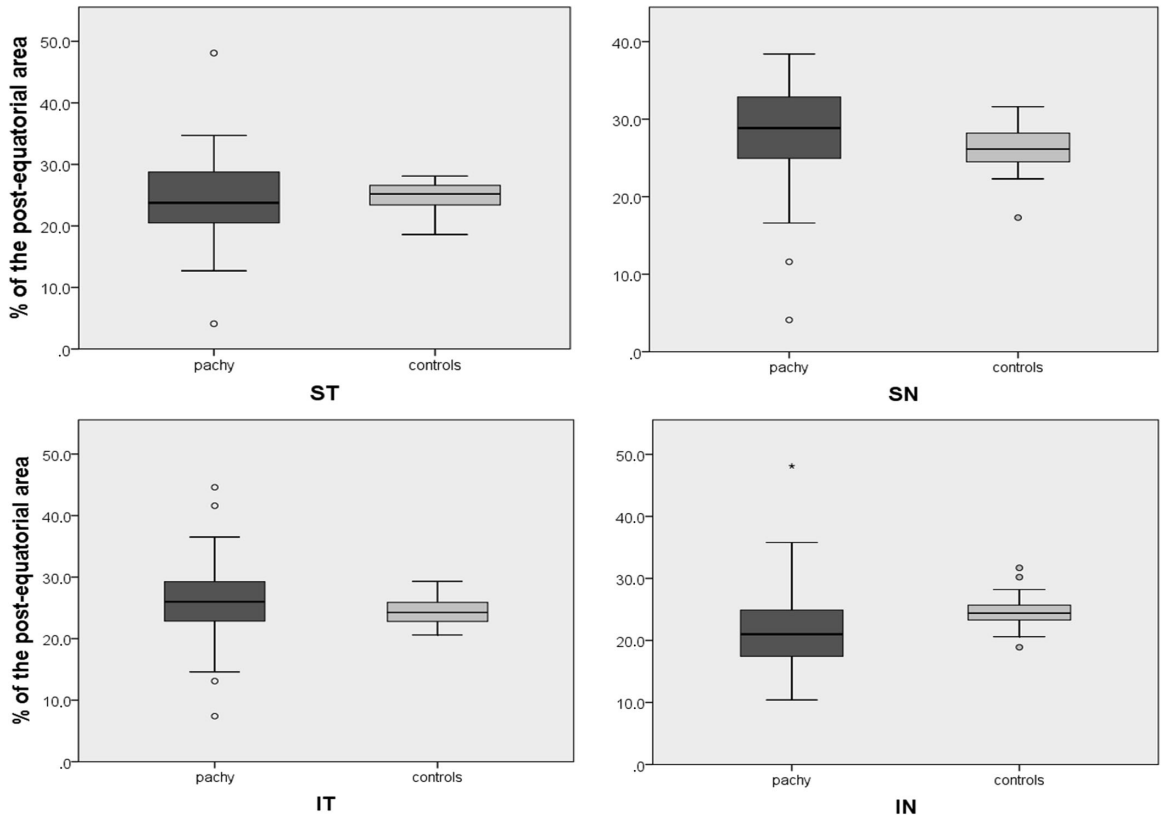

Figure 3. Box and whiskers plots showing median and interquartile range for drainage areas of major vortex vein systems in each quadrant, expressed as percentages of the postequatorial fundus. Note the greater variability of the pachychoroid disease group (pachy; *dark gray boxes*) compared to the control group (controls; *light gray boxes*).

Table 2. Ultra-widefield Indocyanine Green Angiography Characteristics of Pachychoroid and Control Group

	Pachychoroid	Controls	*P* Value
VV drainage areas			
ST (% of the postequatorial area; mean ± SD)	24.3 ± 7.0	24.9 ± 2.0	0.597
IT (% of the postequatorial area; mean ± SD)	26 ± 6.6	24.3 ± 2.1	0.101
IN (% of the postequatorial area; mean ± SD)	21.7 ± 6.6	24.7 ± 2.8	**0.009**
SN (% of the postequatorial area; mean ± SD)	28.0 ± 6.5	26.2 ± 2.8	**0.025**
P	**<0.0001**	.111	
CVH			
N° of eyes showing CVH	52/52 (100.0%)	3/26 (11.5%)	**<0.0001**
ST (n° of CVH spots; mean ± SD)	1.52 ± 1.8	0	
IT (n° of CVH spots; mean ± SD)	1.81 ± 1.8	0.11 ± 0.4	
IN (n° of CVH spots; mean ± SD)	0.23 ± 0.5	0.04 ± 0.2	
SN (n° of CVH spots; mean ± SD)	0.38 ± 0.7	0	
P	**<0.0001**	.284	
Intervortex venous anastomoses			
N° of eyes showing intervortex venous anastomoses	46/52 (88.5%)	9/26 (34.6%)	**<0.0001**
ST (n° of interVV anastomoses; mean ± SD)	1.79 ± 1.4	0.5 ± 0.9	
IT (n° of interVV anastomoses; mean ± SD)	1.73 ± 1.4	0.3 ± 0.7	
IN (n° of interVV anastomoses; mean ± SD)	0.58 ± 0.8	0.2 ± 0.6	
SN (n° of interVV anastomoses; mean ± SD)	1.05 ± 0.9	0.3 ± 0.6	
P	**<0.0001**	*.448*	

SD, standard deviation.

Table 3. Correlation Between Biomarkers of Choroidal Venous Congestion (Choroidal Vascular Hyperpermeability and Intervortex Venous Anastomoses) and the Drainage Area Size of Vortex Vein Systems in Each Quadrant

	CVH Spot Density	Intervortex Venous Anastomoses
ST VV Drainage Area		
r	0.448	0.184
P	**0.001**	0.193
IT VV Drainage Area		
r	0.341	−0.111
P	**0.018**	0.434
IN VV Drainage Area		
r	0.068	0.523
P	0.645	**<0.0001**
SN VV Drainage Area		
r	0.369	0.218
P	**0.011**	0.120

SD, standard deviation.

positive correlation with the size of VV drainage areas in the ST, IT and SN quadrants in the pachychoroid disease group (Table 3). This correlation was not statistically significant in the IN quadrant. CVH was present in 69.3% quadrants with VV drainage areas in the top quartile range and 13.5% quadrants with VV drainage areas in the lower quartile range (4.1%–20.5%). Sites of CVH at the posterior pole were located in areas showing the greatest choroidal thickness as measured by SS-OCTA (Fig. 4) or at the margin of these areas.

Quantification of intervortex venous anastomoses showed inconsistent reproducibility (Supplementary Table S1). A total of 134 and 18 intervortex venous anastomoses were found in eyes with pachychoroid disease and controls, respectively. Intervortex venous anastomoses were present in 46 of 52 (88.5%) of eyes with pachychoroid disease and nine of 26 (34.6%) of control eyes ($P < 0.0001$). In eyes with pachychoroid disease, the most common intervortex venous anastomoses occurred between the ST and IT vortex vein systems (68 [50.7%]) (Fig. 5B), followed by intervortex venous anastomoses between the SN and the ST vortex vein systems (23 [17.2%]) and between the IN and SN vortex vein systems (19 [14.2%]). The IN vortex vein system was the least involved in intervortex venous anastomoses in the pachychoroid disease cohort (30; mean value, 0.58 ± 0.8) and control eyes (7; mean value, 0.2 ± 0.6). The number of intervortex venous anastomoses formed by each vortex vein system did not show a significant correlation with the size of the VV drainage area in each quadrant, except for the IN vortex vein system, for which a positive correlation was demonstrated (Table 3). Intervortex venous anastomoses were commonly seen in areas of maximal choroidal thickness as evaluated by SS-OCT (Fig. 5C).

Choroidal Thickness Analysis

The mean subfoveal choroidal thickness in pachychoroid disease eyes was 390.7 ± 126.5 µm. Widefield SS-OCT volume scans were obtained in 48 pachychoroid disease eyes. Among these OCT volumes, 16 were excluded due to insufficient scan quality including non-optimal segmentation of the choroid-scleral junction. A total of

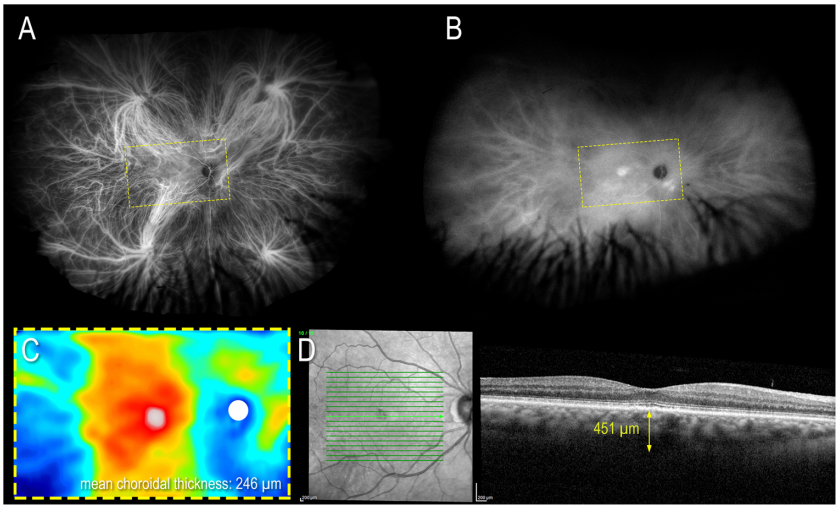

Figure 4. (**A**) Early to mid-phase UW-ICGA of the right eye of a 62-year-old woman with pachychoroid pigment epitheliopathy showing imbalanced choroidal drainage of the postequatorial area due to relative hypoplasia of the inferonasal vortex vein system. The superonasal vortex vein drainage area is enlarged, including a significant portion of the peripapillary area. (**B**) Late phase UW-ICGA of the same eye showing choroidal hyperpermeability spots in the macular and inferonasal peripapillary regions. The *yellow dashed boxes* in **A** and **B** indicate the location of the choroidal thickness map displayed in **C**. (**C**) A 15 × 9 mm swept-source optical coherence tomography thickness map obtained segmenting the choroid between the Bruch's membrane and the choroid-scleral junction. Note that sites of choroidal hyperpermeability as visualized in **B** correspond to areas of maximal choroidal thickness in the macular region that are within the superonasal vortex vein drainage area. (**D**) Spectral-domain optical coherence tomography B-scan passing through the foveal region demonstrating a nonvascularized shallow irregular pigment epithelial detachment colocalizing with the point of maximal choroidal thickness located subfoveally.

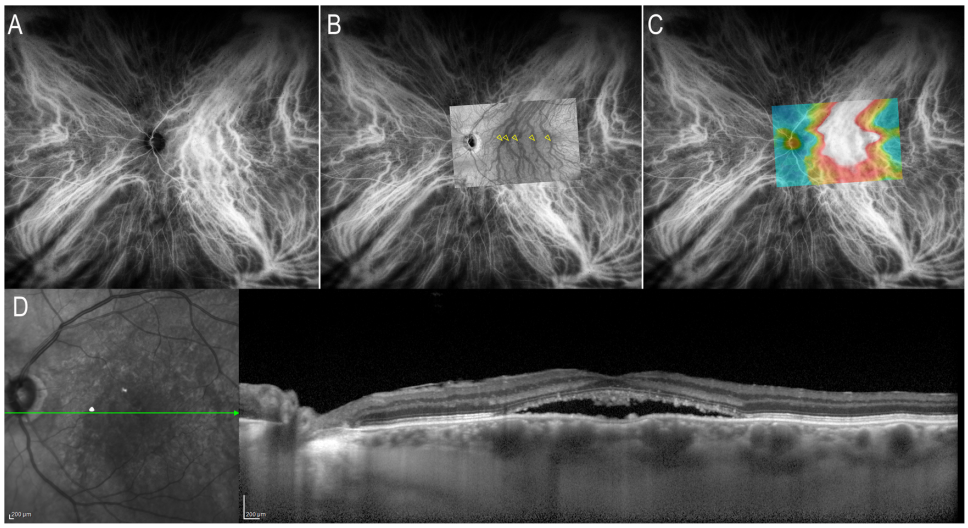

Figure 5. (**A**) Early to mid-phase UWF ICGA image of the left eye of a 60-year-old man with complex central serous chorioretinopathy. (**B**) The 15 × 9 mm SS-OCT en face projection aligned to the same UWF ICGA image as in **A**, demonstrating large intervortex venous anastomoses between the superotemporal and inferotemporal vortex vein systems (*yellow open arrowheads*). (**C**) Color-coded en face SS-OCT choroidal thickness map corresponding to the en face SS-OCT projection in **B**, showing intervortex venous anastomoses present in the macular region with maximal choroidal thickness. (**D**) Spectral-domain optical coherence tomography B-scan passing through the fovea showing a subfoveal neurosensory detachment and cross-sections of enlarged choroidal veins that occupy the full-thickness choroid.

32 widefield SS-OCT studies from pachychoroid cases were analyzed (3 [9 mm × 9 mm] scans, 16 [15 mm × 9 mm] scans, 11 [12 mm × 12 mm] scans, 2 [15 mm × 15 mm] scans). The mean choroidal thickness in the scanned areas was 289.9 ± 66.7 µm (range, 179.9–462.2 µm). The mean choroidal thicknesses corresponding to the IT and ST VV drainage areas were 285.2 ± 86.5 µm and 301.8 ± 62.9 µm, respectively (P = 0.39). Nineteen of 32 (59%) scans demonstrated asymmetric choroidal venous drainage of the macular region, with dominance of a single vortex vein system (Fig. 6B). In 3 eyes the area scanned with SS-OCT was completely drained by a single vortex vein system (the IT in two cases and the ST in one case). The remaining 16 eyes had a dominant vortex vein system draining most of the scanned area (the IT and the ST systems were dominant in seven and nine eyes, respectively). Mean choroidal thickness corresponding to areas drained by

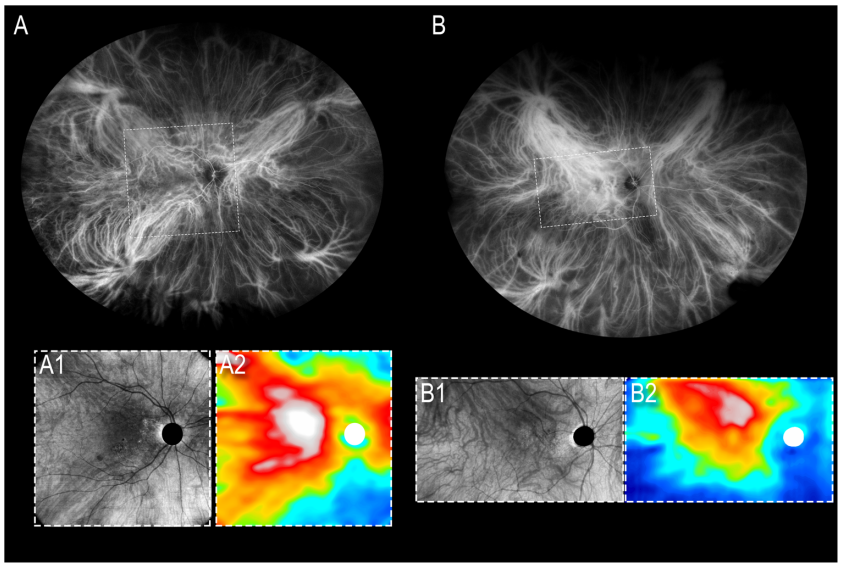

Figure 6. (**A**) Early to mid-phase UWF ICGA image of the left eye of a 57-year-old man with complex central serous chorioretinopathy showing imbalanced choroidal venous drainage due to an inferonasal vortex vein system that is much smaller than those in the other quadrants. The macula is symmetrically drained by the superotemporal and inferotemporal vortex vein systems. The *dasbed box* indicates the location of the SS-OCT scan and thickness map displayed in A1, A2. A1 and A2: 15 × 15 mm SS-OCT en face projection segmenting the choroid. The color-coded choroidal thickness map demonstrates that the region with maximal choroidal thickness in the scanned area corresponds to the proximal extensions of the superotemporal and inferotemporal vortex vein drainage areas. (**B**) Early to mid-phase UWF ICGA image of the left eye of a 75-year-old woman with complex central serous chorioretinopathy showing imbalanced choroidal venous drainage due to small inferior vortex vein systems. The macular drainage is asymmetric as the superotemporal vortex vein system is draining the macular region in its entirety. The *dasbed box* indicates the location of the SS-OCT scan and thickness map displayed in B1, B2. B1 and B2: 15 × 9 mm SS-OCT en face projection segmenting the choroid. The corresponding color-coded choroidal thickness map demonstrates asymmetric distribution of choroidal thickness in the macular region, because the thickest point corresponds to enlarged vessels of the superotemporal vortex vein system.

dominant and non-dominant vortex vein systems was 312.6 ± 75.5 µm and 242.2 ± 75.5 µm, respectively ($P = 0.009$). Vortex vein systems with dominant and non-dominant macular drainage were draining averaged 33.1% (range, 27.2%–48.1%) and 17.1% (range, 4.1%–25.3%) of the postequatorial choroid, respectively. In all eyes with asymmetric drainage of the macular region, the thickest choroidal region was within the dominant VV drainage area, whereas choroidal thickness corresponding to the nondominant VV drainage area was markedly thinner. In eyes with symmetric drainage, choroidal thickness was evenly distributed between the ST and IT VV drainage areas (Fig. 6A).

Discussion

To explore possible mechanisms associated with choroidal venous insufficiency in patients with pachychoroid disease, we sought to determine if affected eyes show greater variability in the area of postequatorial fundus drained by the major vortex vein systems in each quadrant, compared to normal eyes of healthy subjects. We found that eyes with pachychoroid disease had a significant within-subject variance in the size of VV drainage areas. In contrast, a more balanced pattern of choroidal venous drainage was observed in eyes of healthy controls. CVH was present in all eyes with pachychoroid disease but was rarely detected in normal eyes. In pachychoroid disease eyes, sites of CVH were more abundant in the temporal quadrants and were most prevalent in the larger VV drainage areas. While intervortex venous anastomoses were present in 88.5% of the pachychoroid disease cohort, they were also seen in 34.6% of control eyes. When present, intervortex venous anastomoses primarily involved the temporal vortex vein systems. Widefield SS-OCT volume scans centered on the fovea revealed asymmetric choroidal venous drainage of the macular region in 59% of pachychoroid disease cohort. In these eyes, the drainage area of the dominant vortex vein system had the greatest choroidal thickness. In regions scanned with SS-OCT, CVH and intervortex venous anastomoses were more prominent in areas showing greater choroidal thickness.

Based on fluorescein angiographic studies of choriocapillaris filling, Hayreh[45] illustrated the segmental organization of choroidal venous systems, consisting of four quadrants separated by two watershed zones (an horizontal one passing through the disc and fovea, and a vertical one passing through the papillomacular region) and draining into the ST, IT, IN, and SN vortex veins. As a consequence of this organization, vortex vein systems in each quadrant are functionally independent and normally drain roughly equal portions of the choriocapillaris. The major choroidal veins draining the posterior pole gradually increase in caliber during their path towards the periphery, where they converge at vortex vein ampullas. Vortex veins ultimately exit the eye through oblique canals in the sclera. Mechanisms of neural regulation act on top of this spatial arrangement to mitigate the effects of variations of blood inflow in response of retinal activity, fluctuations in the systemic blood pressure driving choroidal perfusion, and possibly retinal temperature.[46]

Vortex vein ampullas and the intrascleral portion of vortex veins have been proposed as sites of choroidal outflow regulation through flow resistance modulation and implicated in mechanisms producing choroidal venous

congestion in pachychoroid disease entities.[33,47] Supporting this hypothesis is the finding of increased scleral thickness in CSC eyes compared to normal eyes that could limit both choroidal venous outflow and transscleral fluid resorption.[48,49]

Under physiological conditions, upregulation of choroidal venous outflow would be limited by the nonexpansible intrascleral path of the vortex veins. Hence, mechanisms producing excess blood volume entering one or more vortex vein systems could be important contributors to sectorial choroidal venous congestion. Variations in choroidal venous drainage from the general schematic described by Hayreh do exist. Mori et al.[50] provided ICGA evidence of asymmetric venous drainage in the choroid of about one half of healthy individuals. Hiroe and Kishi[27] found that the venous drainage of the macular region as evaluated using 12 × 9 mm SS-OCT en face projections was asymmetric in 38% of normal eyes and in 100% of eyes with CSC. Similarly, Hoshino et al.[51] showed that intervortex venous anastomoses and shifting of the horizontal watershed zone were frequently detected in macula-centered wide-field SS-OCT en face images of normal eyes. These authors also speculated that healthy eyes presenting with intervortex venous anastomoses may have subclinical forms of choroidal venous congestion.[51]

A spatial imbalance in choroidal venous drainage may arise in the context of the physiological interindividual variability that characterizes the vascular anatomy of the choroid. One possibility is that a developmental condition such as the relative hypoplasia of one or more vortex vein systems (e.g., the IN vortex vein, as frequently observed in the present series) could promote a misdirection of venous outflow from choriocapillaris portions in the macular/peripapillary regions and alter the physiologic geometry of choroidal venous watersheds. It is possible that a spatial imbalance in choroidal venous drainage may produce an overload of vortex vein systems draining large portions of choriocapillaris, especially from the macular region, where the blood flow is supposed to be maximal. We hypothesize that this imbalanced distribution of choroidal venous drainage may represent an anatomic predisposition to pachychoroid disease rather than a pathogenic determinant per se. In fact, eyes with imbalanced choroidal venous drainage may be more prone to develop choroidal venous congestion as a consequence of vortex vein system overload. This sectorial overload could be counterbalanced by mechanisms of blood redistribution including vascular remodeling and intervortex venous anastomosis formation, similar to that observed after iatrogenic occlusion of vortex veins.[32] The sporadic detection of CVH and intervortex venous connections in apparently healthy eyes may suggest the existence of subclinical forms of choroidal venous insufficiency. In cases where a steady state of subclinical engorgement is altered due to the exhaustion of compensating mechanisms or intervening factors (e.g., corticosteroid intake in predisposed individuals), eyes may develop the clinical sequelae that characterize the different phenotypes within the pachychoroid disease spectrum.

According to our results, the disproportionate drainage through nasal vortex vein systems is the most frequent pattern of choroidal venous drainage imbalance in eyes with pachychoroid disease. In their 2004 study, Mori and coworkers[50] found that the preferential drainage route in healthy eyes with asymmetric macular drainage was the ST vortex vein system in 67% of cases, the IT in 17% and the SN in 17%. Consistent with our findings, the IN was the vortex vein system with smallest drainage area, in any case responsible for the choroidal drainage of the macular region. In a study by Lee et al.,[39] differences in choroidal vascular density between eyes with CSC/thick choroid-PCV and eyes with AMD/thin choroid PCV as evaluated after binarization of UWF ICGA images were significant in all quadrants except for the IN quadrant, suggesting that this vortex vein system may be the less prone to develop choroidal venous congestion. These findings are in line with the low frequency of intervortex venous anastomoses and CVH involving the IN quadrant in our cases. Nevertheless, the patterns of asymmetric choroidal venous drainage in pachychoroid eyes appear to be variable, because, in several cases, the choroidal venous drainage imbalance was due to disproportionate drainage through temporal vortex vein systems, rather than the nasal ones. Regardless, biomarkers of choroidal venous congestion and pathologic features of pachychoroid disease affecting the RPE and the neurosensory retina are more frequent in the temporal quadrants and particularly at the posterior pole. The reasons for that remain speculative and possibly related to the high metabolic demand in the macula, which is usually drained by the temporal vortex vein systems.

We cannot exclude that, at least in some cases, an apparent imbalance of choroidal venous drainage may be the result of acquired alterations secondary to remodeling of drainage routes and intervortex venous anastomosis formation. However, in the present analysis, the boundaries identifying the drainage areas of different vortex vein systems were systematically placed where the posterior terminations of large choroidal veins were clearly visible. In rare cases in which a distinct demarcation line between two vortex vein systems could not be drawn due to abundant intervortex venous anastomoses (e.g., the ST and IT vortex vein systems in the eye shown in Fig. 5), the boundary separating contiguous vortex vein systems was set at the theoretical position of the physiologic watersheds. Moreover, vortex vein systems with large drainage areas did not show greater tendency to form intervortex venous anastomoses compared to small vortex vein systems, suggesting that vascular remodeling was not a major cause of their relative enlargement. In addition, one could expect that an acquired alteration of the choroidal venous system morphology secondary to vascular remodeling should be time-dependent and, therefore, more frequent in old individuals. Actually, patients with pachychoroid disease and at least one VV drainage area in the upper quartile range were not significantly older than the remaining population. This is consistent with the report by Mori et al.,[50] in which development of preferential choroidal drainage routes in normal eyes appeared not attributable to aging. Of note, several eyes from the present series had unusual geometry of choroidal drainage that seemed unlikely to be originating from a balanced drainage organization consistent with Hayreh's model (e.g., Fig. 7).

We acknowledge that the proposed mechanism possibly leading to choroidal congestion may not be relevant in every case. Some pachychoroid disease eyes from the present series did not show evident imbalance of choroidal venous drainage and these eyes usually had diffuse choroidal congestion involving all four quadrants. We surmise that the mechanisms producing choroidal congestion in these cases may be different and possibly related to generalized overload and/or outflow obstruction involving all major vortex vein systems simultaneously.

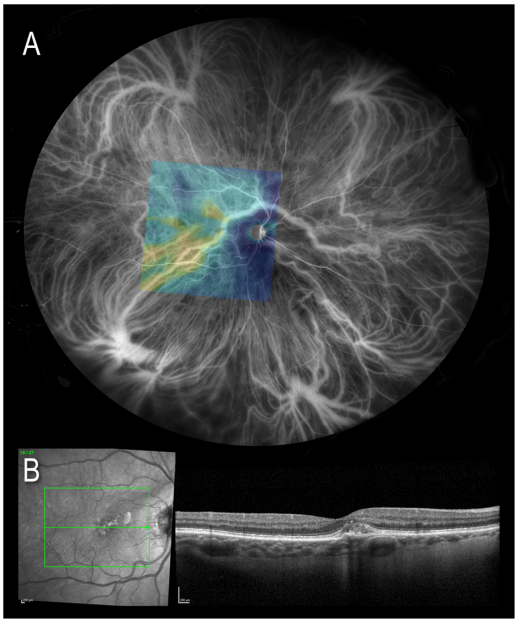

Figure 7. (**A**) Early to mid-phase UWF ICGA image of the left eye of a 72-year-old woman with pachychoroid pigment epitheliopathy. A 12 × 12 mm color-coded swept-source optical coherence tomography choroidal thickness map is aligned and superimposed over the UWF ICGA image and shows an overall thin choroid at the posterior pole. Areas of increased choroidal thickness correspond to large caliber vessels draining into the inferotemporal vortex vein. A very large venous trunk draining the nasal periphery is collecting into the inferotemporal vortex vein system after traversing the macular region. (**B**) Spectral-domain optical coherence tomography B-scan passing through the fovea demonstrates a nonvascularized shallow RPE detachment associated with overlying outer retinal disturbances. Note that RPE and outer retinal alterations are in the immediate proximity to the cross-sectioned, enlarged choroidal vein crossing the macular region.

This study has several limitations. First, its retrospective nature did not allow for the comparison of two age- and sex-matched populations. However, multiple linear regression models did not show significant effect of age and gender on the drainage area size of vortex vein systems. Additionally, clinical data possibly affecting the outcomes, such as axial length, were not recorded for many eyes included in the present analysis and could not be evaluated. SD-OCT and SS-OCT scans were not available for the control group. Although UWF ICGA allowed for the assessment of the postequatorial choroidal drainage in its entirety, choroidal venous outflow originating from regions located anteriorly to the vortex vein ampullas was not evaluated. This component may be relevant to promote vortex vein system overload and pachychoroid disease. The cross-sectional design of our study prevented any definite indication supporting the congenital/developmental versus acquired nature of choroidal venous imbalance. Nevertheless, the present analysis demonstrated a significant imbalance of choroidal venous drainage in a fairly large cohort of pachychoroid disease eyes using UWF imaging. In contrast, the distribution of choroidal venous drainage into different quadrants in eyes of healthy controls did not show such variability. The spatial arrangement of venous drainage routes seemed to affect the patterns of choroidal congestion as evaluable by the location of CVH sites and the distribution of choroidal thickness.

An imbalanced choroidal venous drainage into different quadrants may promote a state of chronic choroidal venous insufficiency occurring with congestion of specific vortex vein systems, sector choroidal thickening associated with choroidal venous hyperpermeability and remodeling of venous drainage routes. This may represent a pathophysiologic model influencing pachychoroid disease. Further studies with a larger population and a longitudinal design are needed to confirm our findings, to evaluate the actual incidence of venous drainage imbalance in eyes with pachychoroid disease and in the normal population, and to shed light on mechanisms affecting the spatial organization of choroidal venous drainage.

Acknowledgments

Supported by the Macula Foundation Inc., New York, NY, USA.

Disclosure: **T. Bacci,** None; **D.J. Oh,** None; **M. Singer,** for Allergan (Irvine, CA, USA) (C), Regeneron (NY, USA) (C), Genentech (San Francisco, CA, USA) (C), Eyepoint (Watertown, MA, USA) (C), Novartis (Basel, Switzerland) (C), AGTC (Cambridge, MA, USA) (C), Adverum (Redwood City, CA, USA) (C), Nanoscope (Bedford, TX, USA) (I), Inflammasome (Newton, MA, USA) (I), Aviceda (Cambridge, MA, USA) (i); **S. R. Sadda,** Heidelberg Engineering (Heidelberg, Germany) (C), Optos (Scotland, UK) (C), Centervue (Padova, Italy) (C), Allergan (Irvine, California, USA) (C), Oxurion (Leuven, Belgium) (C), Amgen (California, USA) (C), Apellis (Waltham, MA, USA) (C), Iveric (NY, USA) (C), Bayer (Berlin, Germany) (C), Roche/Genentech (San Francisco, CA, USA) (C), Regeneron (NY, USA) (C), Novartis (Basel, Switzerland) (C), 4DMT (Emeryville, CA, USA) (C), Carl Zeiss Meditec (Dublin, USA) (F), Nidek (Gamagori, Japan) (F), Topcon (Tokyo, Japan) (F), Heidelberg Engineering (Heidelberg, Germany) (F), Optos (Scotland, UK) (F), Centervue (Padova, Italy) (F); **K.B. Freund,** Heidelberg Engineering (Heidelberg, Germany) (C), Carl Zeiss Meditec (Dublin, USA) (C), Allergan (Irvine, CA, USA) (C), Bayer (Berlin, Germany) (C), Genentech (San Francisco, CA, USA) (C), Regeneron (NY, USA) (C), and Novartis (Basel, Switzerland) (C), Genentech/Roche (San Francisco, CA, USA) (F)

References

1. Warrow DJ, Hoang QV, Freund KB. Pachychoroid pigment epitheliopathy. *Retina.* 2013;33:1659–1672.
2. Pang CE, Freund KB. Pachychoroid neovasculopathy. *Retina.* 2015;35:1–9.
3. Pang CE, Freund KB. Pachychoroid pigment epitheliopathy may masquerade as acute retinal pigment epitheliitis. *Invest Ophthalmol Vis Sci.* 2014;55:5252.
4. Balaratnasingam C, Lee W-K, Koizumi H, Dansingani K, Inoue M, Freund KB. Polypoidal choroidal vasculopathy: a distinct disease or manifestation of many? *Retina.* 2016;36:1–8.
5. Phasukkijwatana N, Freund KB, Dolz-Marco R, et al. Peripapillary pachychoroid syndrome. *Retina.* 2018;38:1652–1667.
6. Chung H, Byeon SH, Freund KB. Focal choroidal excavation and its association with pachychoroid spectrum disorders: a review of the literature and multimodal imaging findings. *Retina.* 2017;37:199–221.
7. Sakurada Y, Leong BCS, Parikh R, Fragiotta S, Freund KB. Association between choroidal caverns and choroidal vascular hyperpermeability in eyes with pachychoroid diseases. *Retina.* 2018;38:1977–1983.

Investigative Ophthalmology & Visual Science

8. Spaide RF. Disease expression in nonexudative age-related macular degeneration varies with choroidal thickness. *Retina.* 2018;38:708–716.
9. Imamura Y, Fujiwara T, Margolis R, Spaide RF. Enhanced depth imaging optical coherence tomography of the choroid in central serous chorioretinopathy. *Retina.* 2009;29:1469–1473.
10. Maruko I, Iida T, Sugano Y, Ojima A, Sekiryu T. Subfoveal choroidal thickness in fellow eyes of patients with central serous chorioretinopathy. *Retina.* 2011;31:1603–1608.
11. Maruko I, Iida T, Sugano Y, Ojima A, Ogasawara M, Spaide RF. Subfoveal choroidal thickness after treatment of central serous chorioretinopathy. *Ophthalmology.* 2010;117:1792–1799.
12. Yang L, Jonas JB, Wei W. Choroidal vessel diameter in central serous chorioretinopathy. *Acta Ophthalmol.* 2013;91:e358–e362.
13. Rhodes LA, Huisingh C, Johnstone J, et al. Peripapillary choroidal thickness variation with age and race in normal eyes. *Invest Ophthalmol Vis Sci.* 2015;56:1872.
14. Jin P, Zou H, Zhu J, et al. Choroidal and retinal thickness in children with different refractive status measured by swept-source optical coherence tomography. *Am J Ophthalmol.* 2016;168:164–176.
15. Gattoussi S, Cougnard-Grégoire A, Korobelnik J-F, et al. Choroidal thickness, vascular factors, and age-related macular degeneration: the ALIENOR Study. *Retina.* 2019;39:34–43.
16. Touhami S, Philippakis E, Mrejen S, et al. Topographic Variations of Choroidal Thickness in Healthy Eyes on Swept-Source Optical Coherence Tomography. *Invest Ophthalmol Vis Sci.* 2020;61:38.
17. Cheung CMG, Lee WK, Koizumi H, Dansingani K, Lai TYY, Freund KB. Pachychoroid disease. *Eye.* 2019;33:14–33.
18. Castro-Navarro V, Behar-Cohen F, Chang W, et al. Pachychoroid: current concepts on clinical features and pathogenesis. *Graefs Arch Clin Exp.* 2021;259:1385–1400.
19. Sakurada Y, Fragiotta S, Leong BCS, Parikh R, Hussnain SA, Freund KB. Relationship between choroidal vascular hyperpermeability, choriocapillaris flow density, and choroidal thickness in eyes with pachychoroid pigment epitheliopathy. *Retina.* 2020;40:657–662.
20. Gal-Or O, Dansingani KK, Sebrow D, Dolz-Marco R, Freund KB. Inner choroidal flow signal attenuation in pachychoroid disease: optical coherence tomography angiography. *Retina.* 2018;38:1984–1992.
21. Matsumoto H, Mukai R, Morimoto M, Tokui S, Kishi S, Akiyama H. Clinical characteristics of pachydrusen in central serous chorioretinopathy. *Graefs Arch Clin Exp* . 2019;257:1127–1132.
22. Hayashi K, Hasegawa Y, Tokoro T. Indocyanine green angiography of central serous chorioretinopathy. *Int Ophthalmol.* 1986;9:37–41.
23. Scheider A, Nasemann JE, Lund O-E. Fluorescein and indocyanine green angiographies of central serous choroidopathy by scanning laser ophthalmoscopy. *Am J Ophthalmol.* 1993;115:50–56.
24. Piccolino FC, Borgia L. Central serous chorioretinopathy and indocyanine green angiography. *Retina.* 1994;14:231–242.
25. Prünte C, Flammer J. Choroidal capillary and venous congestion in central serous chorioretinopathy. *Am J Ophthalmol.* 1996;121:26–34.
26. Iida T, Kishi S, Hagimura N, Shimizu K. Persistent and bilateral choroidal vascular abnormalities in central serous chorioretinopathy. *Retina.* 1999;19:508–512.
27. Hiroe T, Kishi S. Dilatation of asymmetric vortex vein in central serous chorioretinopathy. *Ophthalmol Retina.* 2018;2:152–161.
28. Kishi S, Matsumoto H, Sonoda S, Hiroe T, Sakamoto T, Akiyama H. Geographic filling delay of the choriocapillaris in the region of dilated asymmetric vortex veins in central serous chorioretinopathy. *PLoS One.* 2018;13:e0206646.
29. Matsumoto H, Kishi S, Mukai R, Akiyama H. Remodeling of macular vortex veins in pachychoroid neovasculopathy. *Sci Rep.* 2019;9:14689.
30. Matsumoto H, Hoshino J, Arai Y, et al. Quantitative measures of vortex veins in the posterior pole in eyes with pachychoroid spectrum diseases. *Sci Rep.* 2020;10:19505.
31. Matsumoto H, Hoshino J, Mukai R, et al. Vortex Vein Anastomosis at the Watershed in Pachychoroid Spectrum Diseases. *Ophthalmol Retina.* 2020;4:938–945.
32. Takahashi K, Kishi S. Remodeling of choroidal venous drainage after vortex vein occlusion following scleral buckling for retinal detachment. *Am J Ophthalmol.* 2000;129:191–198.
33. Spaide RF, Gemmy Cheung CM, Matsumoto H, et al. Venous overload choroidopathy: a hypothetical framework for central serous chorioretinopathy and allied disorders [published online ahead of print May 21, 2021]. *Prog Retin Eye Res*, https://doi.org/10.1016/j.preteyeres.2021.100973.
34. Choudhry N, Duker JS, Freund KB, et al. Classification and guidelines for widefield Imaging. *Ophthalmol Retina.* 2019;3:843–849.
35. Verma A, Maram J, Alagorie AR, et al. Distribution and location of vortex vein ampullae in healthy human eyes as assessed by ultra-widefield indocyanine green angiography. *Ophthalmol Retina.* 2020;4:530–534.
36. Verma A, Maram J, Alagorie AR, et al. Peripheral extent of the choroidal circulation by ultra-widefield indocyanine green angiography in healthy eyes. *Br J Ophthalmol.* 2021;105:824–828.
37. Pang CE, Shah VP, Sarraf D, Freund KB. Ultra-widefield imaging with autofluorescence and indocyanine green angiography in central serous chorioretinopathy. *Am J Ophthalmol.* 2014;158:362–371.e2.
38. Hirahara S, Yasukawa T, Kominami A, Nozaki M, Ogura Y. Densitometry of choroidal vessels in eyes with and without central serous chorioretinopathy by wide-field indocyanine green angiography. *Am J Ophthalmol.* 2016;166:103–111.
39. Lee A, Ra H, Baek J. Choroidal vascular densities of macular disease on ultra-widefield indocyanine green angiography. *Graefs Arch Clin Exp.* 2020;258:1921–1929.
40. Kim IK, Lee K, Park JH, Baek J, Lee WK. Classification of pachychoroid disease on ultrawide-field indocyanine green angiography using auto-machine learning platform. *Br J Ophthalmol.* 2021;105:856–861.
41. Jung JJ, Yu DJG, Ito K, Rofagha S, Lee SS, Hoang QV. Quantitative assessment of asymmetric choroidal outflow in pachychoroid eyes on ultra-widefield indocyanine green angiography. *Invest Ophthalmol Vis Sci.* 2020;61:50.
42. Jeong A, Lim J, Sagong M. Choroidal vascular abnormalities by ultra-widefield indocyanine green angiography in polypoidal choroidal vasculopathy. *Invest Ophthalmol Vis Sci.* 2021;62:29.
43. Spaide RF, Ledesma-Gil G, Gemmy Cheung CM. Intervortex Venous Anastomosis in Pachychoroid-Related Disorders. *Retina.* 2021;41:997–1004.
44. Chhablani J, Cohen FB, Central serous chorioretinopathy international group. multimodal imaging-based central serous chorioretinopathy classification. *Ophthalmol Retina.* 2020;4:1043–1046.
45. Hayreh SS. Segmental nature of the choroidal vasculature. *Br J Ophthalmol.* 1975;59:631–648.

Investigative Ophthalmology & Visual Science

46. Reiner A, Fitzgerald MEC, Del Mar N, Li C. Neural control of choroidal blood flow. *Prog Ret Eye Res.* 2018;64:96–130.
47. Spaide RF. Choroidal blood flow: review and potential explanation for the choroidal venous anatomy including the vortex vein system. *Retina.* 2020;40:1851–1864.
48. Imanaga N, Terao N, Nakamine S, et al. Scleral thickness in central serous chorioretinopathy. *Ophthalmol Retina.* 2021;5:285–291.
49. Lee YJ, Lee YJ, Lee JY, Lee S. A pilot study of scleral thickness in central serous chorioretinopathy using anterior segment optical coherence tomography. *Sci Rep.* 2021;11:5872.
50. Mori K. Asymmetry of choroidal venous vascular patterns in the human eye. *Ophthalmology.* 2004;111:507–512.
51. Hoshino J, Matsumoto H, Mukai R, et al. Variation of vortex veins at the horizontal watershed in normal eyes. *Graef Arch Clin Exp.* 2021;259:2175–2180.

Investigative Ophthalmology & Visual Science